Nondipole Ionization Dynamics of Atoms in Superintense High-Frequency Attosecond Pulses

M. Førre,[1] J. P. Hansen,[1] L. Kocbach,[1] S. Selstø,[1] and L. B. Madsen[2]

[1]*Department of Physics and Technology, University of Bergen, N-5007 Bergen, Norway*
[2]*Department of Physics and Astronomy, University of Aarhus, 8000 Aarhus, Denmark*

The ionization of $H(1s)$ in superintense, high-frequency, attosecond pulses is studied beyond the dipole approximation. We identify a unique nondipole 3rd lobe in the angular distribution of the ejected electron and show that this lobe has a well-defined classical counterpart. The ionization is likely to occur in the direction opposite to the laser propagation direction, which is fully understood from an analysis of the classical dynamics.

PACS numbers: 42.50.Hz, 32.80.Fb, 32.80.Rm

The production of short, high-intensity, high-frequency electromagnetic pulses is currently being pursued along two different avenues. First, large-scale free-electron (FEL) and x-ray FEL laser projects aim at producing pulses of hard radiation of ~100 fs duration. Second, advances in laser technology have led to the production of isolated XUV pulses of a duration of only 250 attoseconds [1]. These developments mean that the counterintuitive high-intensity, high-frequency phenomena of atomic stabilization with decreasing ionization probability or rate for increasing intensity [2] may become subject to experimental investigations. Naturally, these prospects have revived the theoretical interest in the study of nonperturbative driving of atomic and molecular systems by high-intensity, high-frequency fields [3–5].

In fully three-dimensional nondipole wave packet calculations [3], we identified the onset of stabilization by a transition from multiphotonlike ionization to ionization dominated by nonadiabatic shakeoff as represented by a lack of overlap between the field-free and field-dressed states and with the emergence of characteristic low-energy electrons. In this Letter, we consider the first fully three-dimensional angular distributions in the high-frequency nondipole regime. In particular, we show that the distributions, which typically have a p-like structure for low intensities, have a characteristic three-lobed shape in intense fields. Furthermore, in the nondipole regime, the ionization is likely to occur antiparallel with the laser propagation direction, which is opposite to what is predicted in intense low-frequency fields [6]. Supported by classical calculations we develop a model that explains the emergence of the unique extra lobe in the angular distributions.

The nonrelativistic dynamics of atoms interacting with a classical electromagnetic field is governed by the time-dependent Schrödinger equation [atomic units (a.u.), $m_e = e = \hbar = a_0 = 1$ are used throughout], $i\partial_t \Psi(r, t) = [\frac{1}{2} \times (p + A)^2 + V(r)]\Psi(r, t)$, with the vector potential $A(\eta)$, $\eta = \omega t - k \cdot r$ and potential V. We consider a linearly polarized laser pulse with wave vector $k = k\hat{z}$, corresponding to the vector potential

$$A(\eta) = \frac{E_0}{\omega} f(\eta) \sin(\eta + \phi)\hat{x}, \qquad (1)$$

with E_0 the electric field amplitude, ω the laser frequency, $f(\eta)$ the laser pulse envelope, ϕ the carrier-envelope phase, and $\hat{x}$ the polarization direction.

The Kramers-Henneberger (KH) form of the light-atom interaction Hamiltonian is useful for numerical ionization studies of atoms in intense, high-frequency fields. We apply the nondipole KH transformation [3,7], $\Psi_{KH} = \exp(i\alpha \cdot p)\Psi$, to the wave function and impose the Coulomb gauge restriction $\nabla \cdot A = 0$ on the field. The vector $\alpha(\eta) \equiv \frac{1}{\omega} \int_{\eta_i}^{\eta} d\eta' A(\eta')$ represents the position relative to the laboratory frame of a classical free-electron in the field. The transformation results in the Hamiltonian [3]

$$H_{KH} = \frac{1}{2} p^2 + \frac{1}{2} A^2 + V(r + \alpha) + \frac{1}{2c^2}(A \cdot p)^2$$
$$- \frac{i}{2c^2} E \cdot p + \frac{1}{c}(A \cdot p)(\hat{z} \cdot p), \qquad (2)$$

where $E = -\partial_t A$ is the electric field. The last three terms which stem from the transformation of the kinetic energy operator, are of relativistic order and vanish in the dipole approximation. The last two oscillate with alternating sign and are expected to have a negligible effect on the electron dynamics. The first is quadratic in A and p and hence always positive, but nevertheless we also expect the effect of this term to be small: it plays the role of a kinetic energy operator in the dynamics and is less than a factor $E_0^2/(\omega^2 c^2)$ as important as the the ordinary p^2 operator in (2). Furthermore, for very high intensities the electron essentially follows the motion of a free-electron in the field, which, within the KH frame of reference, means that the momentum distribution of the electronic wave packet is strongly centered about zero in the polarization direction. Therefore (2) can be approximated by

$$H_{KH} = \frac{1}{2} p^2 + \frac{1}{2} A^2(\eta) + V(r + \alpha(\eta)), \qquad (3)$$

which is valid provided $E_0^2/(\omega^2 c^2) \ll 1$, i.e., in the non-relativistic case. We confirmed the validity of (3) for three

different laser frequencies, $\omega = 0.5$, 1, and 2 a.u., by numerical integration of the time-dependent Schrödinger equation for 5 periods of the field with and without the last three terms of (2). The overlaps of the wave functions were more than 99%, for field strengths up to $E_0 = 10$, 30, and 100 a.u., respectively, for the three frequencies. The spatial dependence of $\boldsymbol{\alpha}$ was also examined, and we confirmed that for the present field parameters all nondipole effects are, in effect, incorporated via the A^2 term. Accordingly, we apply the Hamiltonian (3) in our present study of the nondipole ionization dynamics of H, with focus on the angular distribution of the photoelectron. The ground state is exposed to a 3–15-cycle laser pulse of the form (1) with $f(\eta) = \sin^2(\frac{\pi\eta}{\omega T})$, and central frequency $\omega = 2$ a.u. (23 nm), i.e., pulse durations between 228 and 1140 attoseconds. For the frequency considered here, nondipole effects become important when the electric field strength exceeds 20 a.u. [3,8].

Figure 1 shows a typical example of the probability density distribution of the wave function in the dipole and nondipole descriptions. The snapshots are taken before the pulse, in the middle of the pulse, and at 25 a.u. after the end of the pulse. The displacement in the nondipole case of the wave packet in the propagation direction during the pulse is a manifestation of the classical "figure-eight" motion of a free-electron in the nondipole field. This motion is composed of a velocity component in the propagation direction, superimposed on the ordinary wiggle motion along the laser polarization direction. The drift in the propagation direction can be associated with the action of the magnetic field on the quivering electron. To see this, consider the Lorentz forces on a free-electron in the electromagnetic field. To lowest order in z/c the magnetic force acting along the propagation direction becomes $F_z(t) = -A_x(t)E_x(t)/c$. Then, for an electron that is ini-

tially at rest, the velocity in this direction is $v_z(t) = A_x^2(t)/(2c)$, which is indeed never negative. For this reason, one might expect that the ionized electron has a velocity component along the positive z axis after the pulse has passed. This is, however, not necessarily the case since $v_z = 0$ at the end of the pulse. In fact, the electron is most likely ejected oppositely to the propagation direction. The last snapshot in Fig. 1 clearly shows this trend. The up/down asymmetry follows from the interplay between the electromagnetic and Coulombic forces during the pulse. The electromagnetic forces alone do not change the electron momentum along the propagation direction at the end of the pulse, since $v_z(T) = 0$. On the other hand, the net effect of the Coulomb forces on the polarized charge cloud is a momentum component along the negative z axis: the electron, which is most probably situated in the upper hemisphere during the pulse, gets a momentum kick in the negative z direction each time it passes close to the nucleus.

To clarify this point further, we have plotted the dipole and nondipole angular distributions of the continuum electron in Fig. 2. The data are taken for $E_0 = 30$ a.u. and pulses with 3, 5, 10, and 15 cycles, respectively. The horizontal axis (x axis) indicates the laser polarization direction, and the pulse propagates in the positive z direction (upwards). The left/right asymmetry in the angular distributions reveals that the dynamics is strongly nonadiabatic even for the longest pulse considered here. This means that the shape of the distributions is sensitive to the value of the carrier-envelope phase, ϕ. The data in Fig. 2
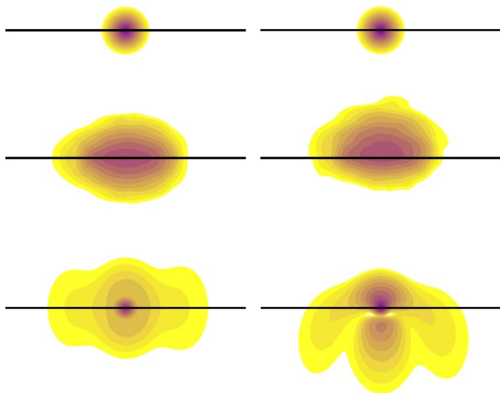

FIG. 1 (color online). Dipole (left) and nondipole (right) probability densities of the KH wave function in the $x - z$ plane for a $\hat{x}$-polarized, 10-cycle pulse propagating in the positive z direction (upward), with $E_0 = 30$ a.u., $\omega = 2$ a.u., and $\phi = 0$. The snapshots are taken at $t = 0$, $t = T/2$, and $t = T + 25.1$ a.u. with $T = 31.4$ a.u.. The length of the horizontal line corresponds to 50 a.u.. The scale is logarithmic with four contours per decade.
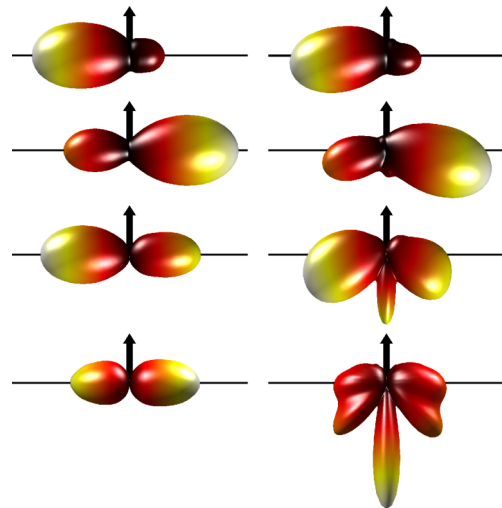

FIG. 2 (color online). Dipole (left) and nondipole (right) electron angular distributions for a 3- (upper), 5- (second), 10- (third), and 15-cycle pulse (lower panel) linearly polarized in the horizontal direction, with $\omega = 2$ a.u., $E_0 = 30$ a.u., and $\phi = 0$. The propagation direction, marked with an arrow, is along the positive z axis. In all cases the total ionization probability lies between 0.4 and 0.5, and the ratios of probability of ionization between the nondipole and dipole cases are 1.00, 1.06, 1.17, and 1.16 for the four different pulses.

were obtained for $\phi = 0$. Figure 3 shows similar spectra for a five-cycle pulse with $E_0 = 20$, 30 and 45 a.u., respectively, but here the data are averaged over the phase ϕ. Both the distributions in Figs. 2 and 3 confirm the features exhibited in Fig. 1. The differential spectra are indeed bent downwards in the nondipole regime, i.e., in the direction opposite to the laser propagation direction. The more intense the pulse, the greater the degree of deflection. In one-photon ionization, this bending of the p-like distribution (see Fig. 2) is a well-known consequence of the nondipole terms proportional to $\boldsymbol{k} \cdot \boldsymbol{r}$. But now the ionization mechanism is completely different: the electron is mainly released into the continuum due to a nonadiabatic adjustment to the time-averaged KH potential, $V_0(\alpha_0; \boldsymbol{r}) = 1/T \int_0^T V(\boldsymbol{r} + \boldsymbol{\alpha}) dt$ [3], where $\alpha_0 \equiv E_0/\omega^2$ is the quiver amplitude. Also, this very different ionization mechanism leads to a new strong field and nondipole feature that is manifested by a characteristic three-lobed shape of the angular distributions. The third lobe in the direction anti-parallel to the propagation direction is not present in the weak-field nondipole regime [9], neither is it present in the dipole limit of strong-field ionization. The extra lobe becomes most distinct for the longest and most intense pulses. For $E_0 = 30$ a.u. it is not visible for the three-cycle pulse, whereas it is prominent for the 10 and 15-cycle pulses. Furthermore, for the case of a five-cycle pulse it becomes important for $E_0 > 30$ a.u.. The three-lobe structure is present for any value of the carrier-envelope phase, but the relative size of the two side lobes can vary a lot for different choices of ϕ.

In order to get a deeper insight into the physical processes governing the observed features, we have performed a classical trajectory Monte Carlo analysis of the problem. The classical angular distributions were obtained from the solutions of the Newtonian equations of motion for a large number ($\sim 100\,000$) of individual electron trajectories with initial conditions taken from a microcanonical ensemble

[10]. Figure 4 (upper) shows the final angular distribution corresponding to those classical electron orbits that are unbound in the nondipole limit but remain bound within the dipole picture. The figure should be compared with the lower right figure in Fig. 3. The one-lobed shape of the distribution is striking. Hence, the classical calculation reveals that the fraction of the wave packet that remains bound within the dipole approximation but is ionized in the nondipole regime contributes to the creation of a third lobe in the spectra.

Both the deflection of the two side lobes and the creation of a new lobe in the angular distributions can in fact be attributed to the very same physical process which is of purely classical origin. In the nondipole regime the inten-
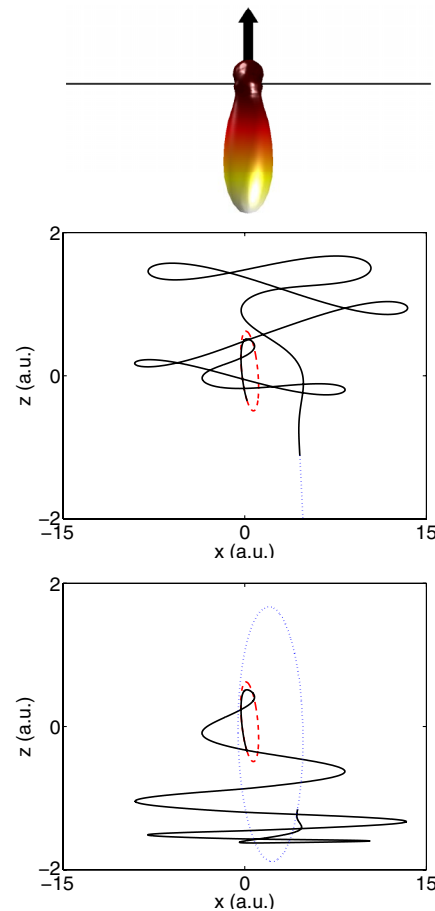
FIG. 4 (color online). Upper panel: Classical angular distribution corresponding to those classical trajectories that remain closed orbits within the dipole approximation but are unbound in the nondipole description. The data, which are averaged over the carrier-envelope phase ϕ, are taken for a five-cycle pulse with $E_0 = 45$ a.u. and $\omega = 2$ a.u.. Middle panel: A single classical trajectory that contributes to the third lobe in the angular distribution. Lower panel: The same trajectory in the dipole approximation. The dashed (red) and dotted (blue) curves indicate the initial and final orbits, respectively, and the full curve (black) shows the trajectories during the pulse. The linear polarization is along the x axis and the pulse propagates in the positive z direction.
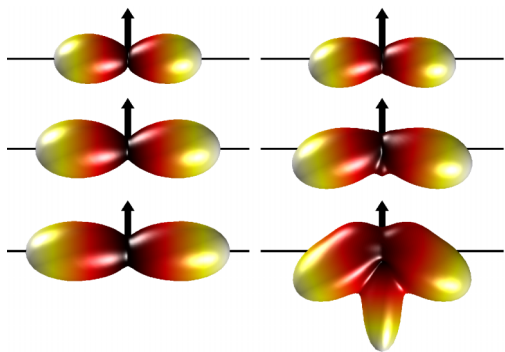

FIG. 3 (color online). As Fig. 2, but for a five-cycle pulse and for three different field strengths, $E_0 = 20$ (upper), $E_0 = 30$ (middle), and $E_0 = 45$ a.u. (lower panel). The data are averaged over the carrier-envelope phase. The total ionization probability is between 0.41 and 0.63, and the ratios of probability of ionization between the nondipole and dipole cases are 1.01, 1.06, and 1.20 for the three different pulses.

sity of the laser is so high that the electron essentially follows the motion of a classical free-electron in the field. However, the electron will accumulate momentum from a series of Coulomb scattering events during the pulse. The momentum kicks imparted to the electron from these events may eventually lead to ionization. Although the electron receives momentum kicks both in the dipole and nondipole cases there is one important difference in the nondipole situation: because of the figure-eight motion, the electron's orbit is displaced in the propagation direction during the laser pulse, and a classical electron will typically spend more time in the upper hemisphere than in the lower hemisphere. The average effect of the Coulomb forces on the electronic motion in the up/down direction is, accordingly, a net momentum transfer to the electron in the direction opposite to the propagation direction. This explains the up/down asymmetry of the angular distributions in the nondipole regime.

Orbits that contribute to the extra lobe in the angular distributions have one thing in common: they are ionized as a result of an intimate interplay between magnetic, electric and Coulomb forces during the pulse. Because of the magnetic drift motion, the ionizing trajectories very early become confined to the upper hemisphere and the electron will remain there until the end of the pulse, even though it receives momentum kicks in the opposite direction from successive encounters with the nucleus. However, at the end of the pulse, when the magnetic drift motion ceases, the electron is left with a velocity component along the negative z direction. It is this momentum component, which roughly equals the algebraic sum of all such momentum kicks imparted to the electron during the pulse, that finally enables the electron to escape. The creation of the third lobe and the dependence of the three-lobed structure on the pulse duration (see Fig. 3) is understood accordingly. In Fig. 4 (middle and lower panels) we follow one of the single classical trajectories that contributes to the third lobe in the angular distributions in the nondipole case. The differences between the nondipole (middle panel) and the dipole (lower panel) are striking. Within the dipole approximation the electron is transferred to an excited closed orbit by the electric field, whereas the electron is ionized when the spatial dependence of the field is included. This particular example illuminates essentially all the fundamental aspects of the dynamics, i.e., the figure-eight motion, the drift motion, and the quivering motion of the electron.

In contrast to the present dynamics, optical laser frequencies cannot be expected to produce the same third lobe for two reasons. First, the excursion is in this case so large that the intimate interplay between the magnetic and the nuclear force will be much less pronounced. Second, for low-frequency fields the substantial ionization occurs in a fraction of or after only a few optical cycles, so that the "three-lobe ionization mechanism", which is a relatively slow process in the sense that it needs several cycles to be efficient, becomes much less important. In addition, in the stabilization regime the ionized electron typically has a very low kinetic energy and is, therefore, effectively steered by the Coulomb kicks imparted to it. We remark, however, that the ionization mechanism that is responsible for the third lobe also is present for lower frequencies, but that its relative importance very rapidly decreases as the frequency is decreased. Although the effect is strongly suppressed in the ionization of $H(1s)$, it should in principle be possible to measure the third lobe in weakly bound systems with optical laser frequencies, but now additional nondipole effects, due to the extended size of the system compared to the central pulse wavelength, may become important [11].

In conclusion, we obtained the first angular distributions for the photoelectron in the ionization of $H(1s)$ in super-intense, high-frequency, attosecond pulses. Our treatment went beyond the dipole approximation, and we identified a unique signature for the onset of nondipole effects in the spectra. We showed that the common two-lobed shape of the angular distributions in the dipole regime develops gradually into a deflected three-lobed shape in the high-frequency nondipole regime. A detailed classical analysis of the spectra revealed the classical nature of the underlying dynamics.

[1] R. Kienberger *et al.*, Nature (London) **427**, 817 (2004); A. Scrinzi, M. Yu. Ivanov, R. Kienberger, and D. M. Villeneuve, J. Phys. B **39**, R1 (2006).

[2] See, e.g., M. Gavrila, J. Phys. B **35**, R147 (2002); A. M. Popov, O. V. Tikhonava, and E. A. Volkova, J. Phys. B **36**, R125 (2003).

[3] M. Førre, S. Selstø, J. P. Hansen, and L. B. Madsen, Phys. Rev. Lett. **95**, 043601 (2005).

[4] S. Selstø, M. Førre, J. P. Hansen, and L. B. Madsen, Phys. Rev. Lett. **95**, 093002 (2005).

[5] A. Staudt, C. H. Keitel, and J. S. Briggs, J. Phys. B **39**, 633 (2006); A. D. Bandrauk and H. Z. Lu, Phys. Rev. A **73**, 013412 (2006).

[6] Y. I. Salamin, S. X. Hu, K. Z. Hatsagortsyan, and C. H. Keitel, Phys. Rep. **427**, 41 (2006).

[7] W. Pauli and M. Fierz, Nuovo Cimento **15**, 167 (1938); H. A. Kramers, *Collected Scientific Papers* (North-Holland, Amsterdam, 1956), p. 866; W. C. Henneberger, Phys. Rev. Lett. **21**, 838 (1968).

[8] N. J. Kylstra *et al.*, Phys. Rev. Lett. **85**, 1835 (2000).

[9] O. Hemmers, R. Guillemin, and D. W. Lindle, Radiat. Phys. Chem. **70**, 123 (2004).

[10] J. P. Hansen, J. Lu, L. B. Madsen, and H. M. Nilsen, Phys. Rev. A **64**, 033418 (2001); H. M. Nilsen, L. B. Madsen, and J. P. Hansen, *ibid.* **66**, 025402 (2002).

[11] T. Mercouris, Y. Komninos, and C. A. Nicolaides, J. Phys. B **35**, 1439 (2002).